Atmospheric Research 225 (2019) 1–16

Contents lists available at ScienceDirect

Atmospheric Research

journal homepage: www.elsevier.com/locate/atmosres

A MCDM-based framework for selection of general circulation models and projection of spatio-temporal rainfall changes: A case study of Nigeria

Mohammed Sanusi Shiru[a,b], Shamsuddin Shahid[a], Eun-Sung Chung[c,*], Noraliani Alias[a], Laura Scherer[d]

[a] Department of Water and Environmental Engineering, School of Civil Engineering, Faculty of Engineering, Universiti Teknologi Malaysia (UTM), 81310 Johor Bahru, Malaysia
[b] Department of Environmental Sciences, Faculty of Science, Federal University Dutse, P.M.B 7156 Dutse, Nigeria
[c] Department of Civil Engineering, Seoul National University of Science and Technology, 01811 Seoul, Republic of Korea
[d] Institute of Environmental Sciences (CML), Leiden University, Einsteinweg 2, 2333 CC Leiden, the Netherlands

ARTICLE INFO

Keywords:
Feature selection method
General circulation model
Information entropy
Statistical downscaling
Random forest

ABSTRACT

A multi-criteria decision-making approach was used for the selection of GCMs for Nigeria based on their ability to replicate historical rainfall estimated using three entropy-based feature selection methods namely, Entropy Gain (EG), Gain Ratio (GR), and Symmetrical Uncertainty (SU). Performances of four bias correction methods were compared to identify the most suitable method for downscaling and projection of rainfall using the selected GCMs. Random forest (RF) regression was used for the generation of the multi-model ensemble (MME) average of projected rainfall. The ensemble projections for each of the representative concentration pathways (RCPs) 2.6, 4.5, 6.0, and 8.5 were computed and compared with global precipitation climatology centre (GPCC) historical rainfall of Nigeria to assess the percentage changes in annual rainfall with 95% level of confidence at different ecological zones for three future periods 2010–2039, 2040–2069, and 2070–2099. Quantile regression was used to assess the changes in seasonal rainfall at 95% confidence interval over the present century. The results revealed that MRI-CGCM3, HadGEM2-ES, CSIRO-Mk3-6-0 and CESM1-CAM5 are the most suitable GCMs for the projection of rainfall in Nigeria. The linear scaling method was found as the most suitable approach for downscaling of rainfall in terms of all the statistical indices used. It was found to downscale rainfall with normalized root mean square error (NRMSE) in the range of 30.7–44.0%, while Nash-Sutcliff efficiency (NSE) was between 0.81 and 0.91, and modified coefficient of agreement (md) was between 0.82 and 0.88. Projection of rainfall showed no significant change in Nigeria over the century under RCP 2.6, 4.5 and 6.5, while RCP 8.5 showed a decrease in the last part of the century (2070–2099). The seasonal changes in rainfall showed an increase in rainfall in the range of 0–20% in most parts of the north. The methodology in this study can reduce the uncertainty inherent in climate change projection and produce better projection of possible spatial and temporal changes in annual and seasonal rainfall.

1. Introduction

It has been generally accepted that climate change resulting from excessive greenhouse gases emissions has caused increased flooding, severe and more frequent droughts, increased wild fires and heatwaves in various parts of globe (Ahmed et al., 2018a; Shiru et al., 2019). These have increased poverty, loss of lives, damages to properties, and ecosystem degradation in many parts. Projections from the general circulation models (GCMs) have been studied and applied for a long time and are invaluable in developing comprehensive adaptation and mitigation measures for simulated impacts of the changing climate. However, GCMs are faltered by their coarser spatial resolution and the uncertainty in their outputs at monthly or lower timescales, which makes their direct usage in climate change impact studies at local and regional scales undesirable (Xue et al., 2007; Onyutha et al., 2016). The GCMs are therefore required to be downscaled in order to bridge the gap between the resolution of these global models and those of the more policy-relevant regional and local scales (Sa'adi et al., 2017). In practice, a number of appropriate GCMs are selected for the region of interest by excluding those considered very unrealistic in order to reduce uncertainties associated with GCMs (Lutz et al., 2016; Pour et al., 2018). Therefore, selection and downscaling of GCMs are the major

* Corresponding author.
E-mail address: eschung@seoultech.ac.kr (E.-S. Chung).

https://doi.org/10.1016/j.atmosres.2019.03.033
Received 2 December 2018; Received in revised form 21 March 2019; Accepted 22 March 2019
Available online 23 March 2019
0169-8095/

challenge in climate change impact analysis.

There are two general approaches, the past performance and the envelope approach for GCM selection (Salman et al., 2018; Khan et al., 2018a). In the past-performance approach, the climate models are selected based on their ability to simulate the historical climate while an ensemble of models covering a wide range of projections is selected in the envelope approach. Though it cannot be assured that a model that performed well in simulating past climate will be able to simulate future climate with similar exactness, the past performance assessment has been widely used for the selection of GCMs. Furthermore, when the past performances of a whole pool of climate models that covers the whole band of climate projections are assessed to select GCMs, the envelope approach is no more required. A number of filters and wrappers have been used for the past performance assessment (McSweeney et al., 2015; Lutz et al., 2016) which includes various statistical indices, skill metrics, or a combination of those in a multi-criteria decision-making (MCDM) framework. However, most studies assessed the limited performances of GCMs based on mean state of historical rainfall where temporal variability of rainfall is often ignored. Entropy can measure the average information content in one variable about another variable. Thus, the entropy-based approach can be used to rank all considered GCMs based on their ability to simulate annual and seasonal variability of observed rainfall at different grid points. The ranking information at different grid points can be used in a MCDM system for the reliable selection of GCMs as it approves the ability of GCMs to simulate the historical rainfall in terms of both the spatial and temporal variability.

There are two general methods used for rainfall downscaling, dynamical and statistical methods. The statistical downscaling has several advantages over dynamical downscaling like cost effectiveness and computational efficiency, provision of point-scale climatic variables from GCM-scale output, and the ability to directly incorporate observations into methods, and as such have been widely used (Pour et al., 2014; Laflamme et al., 2016; Sachindra et al., 2018). Over the past decades, different statistical downscaling models (SDMs) have emerged and are broadly classified as perfect prognosis (PP) and model output statistics (MOS). In PP, a statistical relationship is established between observed climate variables (predictand) and observed large-scale predictors, this relationship is then used for the future projection of climate variable using GCM simulated predictors (Maraun et al., 2010; Manzanas et al., 2015). In MOS, GCM simulated predictors as opposed to the observe predictors are used in establishing this relationship with observed predictands, then the link is applied to the projection using simulated predictor for a future scenario (Eden and Widmann, 2014; Turco et al., 2017; Ahmed et al., 2018b). Among the two methods, the MOS can explicitly account for inherent error and bias of GCMs, thus, it has been frequently used to downscale climate change scenarios (Eden and Widmann, 2014; Sa'adi et al., 2017). Multi-model ensemble (MME) can be used to reduce uncertainties inherent in climate projections arising from wide variations in projections of different GCMs due to their structural differences (Sachindra et al., 2014; Sa'adi et al., 2017). There are different techniques for the generation of MME among which is the commonly used weighted average method in which the historical relationships between observations and forecasts are used in determining weights (Sanchez-Gomez et al., 2009). The efficiency of ensemble approach is very important for reduction of uncertainties in climate projections. Recent studies reported better efficiency of regression-based MME due to their ability to preserve the changes in mean and variability of ensemble member (Steinschneider et al., 2015; Ishizaki et al., 2017). Data mining methods have higher capability for simulation of regression problem and therefore, they can be used to generate better MME. Uncertainty in rainfall projection is paramount in any climate change adaptation and mitigation planning. Different approaches have been mentioned in literature to assess the uncertainty in rainfall projections (Hertig et al., 2014; Ben Daoud et al., 2016; Lafaysse et al., 2014; Soraisam et al., 2018; Fu et al., 2018). Quantile regression (QR) can be used for reliable assessment of trends in different quantiles of rainfall. The dynamism of the climate is affecting the patterns of rainfall (Thomas and López, 2015; Ahmed et al., 2017a; Nashwan and Shahid, 2018) and temperature (Piao et al., 2010; Salman et al., 2017; Khan et al., 2018b) across the globe and will have more severe implications in the future. Africa is especially vulnerable to climate change (Scherer and Verburg, 2017), and Nigeria in West Africa has been experiencing the brunt impacts of the changing climate such as floods and droughts (Douglas et al., 2008; NEMA, 2012; Shiru et al., 2015; Oloruntade et al., 2017; Shiru et al., 2018). An insight into the variations of the climate in the future and how it will affect future disaster occurrences for the country is therefore paramount to the development of the best planning and mitigation measures for such events. This study involves the use of feature selection methods Entropy Gain (EG), Gain Ratio (GR), and Symmetrical Uncertainty (SU) in ranking a total of 20 GCMs according to their ability to replicate global precipitation climatology centre (GPCC) historical rainfall of Nigeria, after which MCDM was used to finally select the most suitable GCMs to form an ensemble GCM. Statistical downscaling of selected GCMs was conducted to assess the spatial and temporal variation of GPCC rainfall over Nigeria. Four widely used bias corrections approaches were compared to find the most suitable approach using multiple visual and numerical performance criteria. Random forest (RF; Breiman, 2001) regression was used in the computation of the MME average of downscaled rainfall. The percentage changes of annual mean rainfall with 95% level of confidence at different ecological zones of Nigeria during three future periods, 2010–2039, 2040–2069, and 2070–2099 and for all RCPs – RCP 2.6, RCP 4.5, RCP 6.0, and RCP 8.5 were assessed. Besides, the spatial changes in rainfall projections for all RCPs were assessed for the future periods. Finally, QR was used to assess the changes in seasonal monthly rainfall at 95% level of confidence for better informed changes in monthly rainfall for policy planning.

2. Study area and data

2.1. Study area

The area of study, Nigeria, is located in West Africa (Latitudes 4°152–13°552 N; Longitude: 2°402 and 14°452E) and covers an area of 923,000 km^2 (Fig. 1). The Nigerian climatic condition is mainly classified into the rainy and the dry seasons. The rainy season which starts in April through to October in the south have rainfalls occurring at over 2000 mm/yr. In the northernmost parts, the rainfalls are below 500 mm/yr and occur between June and September. The annual, rainy season and dry season rainfalls of Nigeria are given in Fig. 2. Due to the

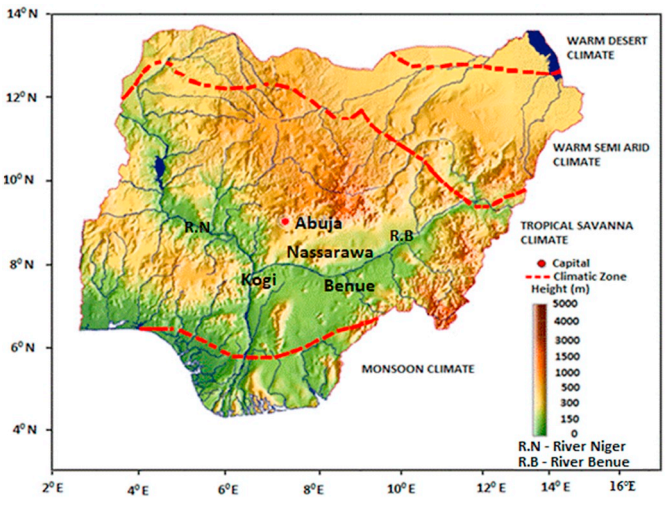

Fig. 1. Climatic zones and topography of Nigeria.

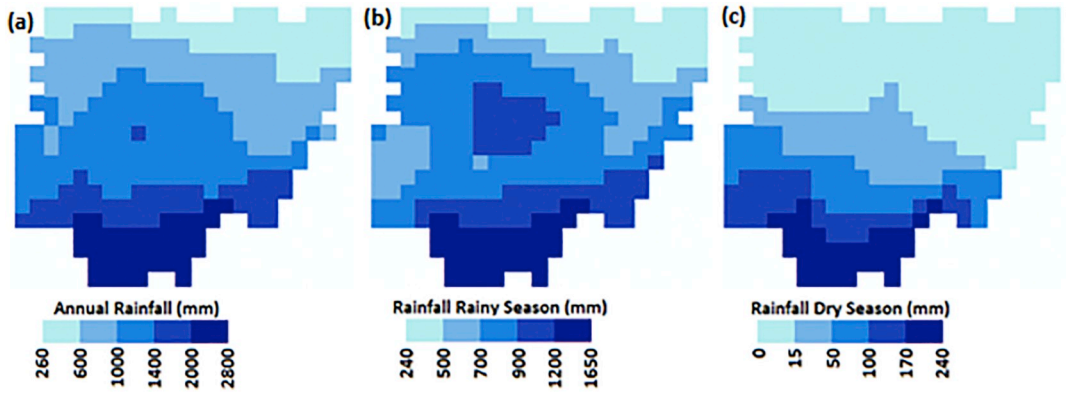

Fig. 2. Spatial distribution (0.5° × 0.5°) of (a) annual; (b) rainy season; and (c) dry season rainfall prepared using monthly GPCC data for the period 1971–2000. Please note that the color scales differ.

variation in the rainy and dry seasons between the north and the south of the country, the common rainy season (June–September), and the common dry season (December–March) are considered for both areas in this study. Temperatures during the dry season in the south range from 30° to 37 °C, while those of the north get to as high as 45 °C in the northeastern parts. The lowest temperatures in the country are recorded during the hazy Harmattan season occurring between December and February. Temperatures during this period are between 17° and 24 °C in the south and reaching 12 °C in the north.

Different ecological zones from the Sahel savanna in the north to the mangrove swamp in the south exist within the country. This is attributable to the varying climatic conditions of the country with the warm desert and semi-arid climate in the north, the tropical savanna climate in the centre, and the monsoon climate in the south (Fig. 1). Elevation ranges from 0 m at the Atlantic Ocean in the south to 2419 m at Chappal Waddi in the north.

2.2. Data

2.2.1. Historical rainfall data

Like most of the developing countries, obtaining reliable climate data in Nigeria is arduous. The distribution of gauges across the country is sparse with currently only 87 operating rain gauges across the country is available as against the 1057 required for appropriate rainfall measurements and attainment of gauge density of 874 km^2 (Ngene et al., 2015) as recommended by the World Meteorological Organization (WMO, 1965). The available stations are also not well distributed over the country. Furthermore, there are incomplete data for some stations which may have implications in climatic studies. Gridded climate data are suggested for climatic studies in such situation. A number of gridded climate data have been developed in recent years owing to the need of the availability of longer term densely distributed climatic data. Though the gauge-based gridded data are developed using observed data, gridded data may be more reliable than the observed data due to careful data analysis and quality control carried out by the developers.

This study uses the GPCC full data reanalysis product of the Deutscher Wetterdienst (Becker et al., 2013; Schneider et al., 2014) as the reference data. The GPCC precipitation reanalysis full data product offers a number of advantages: (1) good data quality for hydrological studies, (2) long time span of data for wider study length, (3) a climate model derived dataset which is based on the highest number of collected precipitation records, (4) completeness of the time series after January 1951 (Spinoni et al., 2014; Ahmed et al., 2015; Ahmed et al., 2017b). This study uses the GPCC monthly rainfall data for the period of 1961–2005 at 323 grid points covering Nigeria.

2.2.2. CMIP5 datasets

The Coupled Model Intercomparison Project phase 5 (CMIP5) is a set of globally coordinated GCM simulations which comprises of historical and future climate simulations assembled from different modeling groups. The CMIP5 offers significant improvements compared to the CMIP3 (Taylor et al., 2012). For this study, 20 monthly simulations of GCMs of the CMIP5 were selected based on the availability of the RCP 2.6, 4.5, 6.0, and 8.5 for Nigeria. The names of the selected GCMs, their modeling centers, and their resolutions are given in Table 1.

3. Methods

An overview of the procedure for the spatial and temporal projection of changes in rainfall for this study is given as follows:

1. Resampling of all 20 selected GCMs to a 2° × 2° grid using bilinear interpolation method and aggregate the GPCC rainfall to the resolution of GCM common resolution (2° × 2°) using area weighted averaging method.
2. Selection of a subset of the 20 GCMs from the CMIP5 using a combination of past performance assessment and envelope approach.
3. *Re*-gridding of selected GCMs to a spatial resolution of GPCC rainfall (0.5° × 0.5°).
4. The use of four bias correction methods and the GPCC rainfall as basis for the bias correction in the GCMs at each GPCC grid point.
5. Selection of best bias correction method and use the method for correction of bias in GCM simulations under the four RCPs for the period 2010–2099.
6. Generation of an ensemble of downscaled GCM projections using RF regression to reduce the dependency on a single GCM to project the future changes in rainfall.
7. The MME rainfall was used for the projection of spatial, temporal and seasonal changes in rainfall for three future periods (2010–2039, 2040–2069, and 2070–2099) against the historical period (1971–2000).
8. QR was used to assess the rainfall changes in summer and winter in different climatic zones of Nigeria for different RCPs at 95% level of confidence.

The following sections discuss the methods used in the selection of the GCMs and the downscaling model development.

3.1. GCM ensemble selection

For reliable climate studies, the selection of the most suitable GCMs is crucial. However, this selection can be very challenging due to the many existing GCMs of various resolutions and degrees of uncertainties from different modeling centers. These uncertainties associated with

Table 1
Basic information about the selected precipitation GCMs.

No	Institution	Model name	Resolution (°, Lon × Lat)
1	Beijing Climate Center, China Meteorological Administration	BCC-CSM1-1	2.8 × 2.8
2		BCC-CSM1.1(m)	1.125 × 1.125
3	National Center for Atmospheric Research, USA	CCSM4	1.25 × 0.95
4		CESM1-CAM5	1.25 × 0.95
5	Commonwealth Scientific and Industrial Research Organization, Australia	CSIRO-Mk3-6-0	1.875 × 1.875
6	The First Institute of Oceanography, SOA, China	FIO-ESM	2.8 × 2.8
7	Geophysical Fluid Dynamics Laboratory, USA	GFDL-CM3	2.5 × 2.0
8		GFDL-ESM2G	2.5 × 2.0
9		GFDL-ESM2M	2.5 × 2.0
10	NASA Goddard Institute for Space Studies	GISS-E2-H	2.5 × 2.0
11		GISS-E2-R	2.5 × 2.0
12	Met Office Hadley Centre, UK	HadGEM2-AO	1.875 × 1.25
13	Met Office Hadley Centre, UK	HadGEM2-ES	1.875 × 1.25
14	Institut Pierre-Simon Laplace, France	IPSL-CM5A-LR	3.75 × 1.875
15		IPSL-CM5A-MR	2.5 × 1.25
16	The University of Tokyo, National Institute for Environmental Studies, and Japan Agency for Marine-Earth Science and	MIROC5	1.4 × 1.4
17	Technology	MIROC-ESM	2.8 × 2.8
18		MIROC-ESM-CHEM	2.8 × 2.8
19	Meteorological Research Institute, Japan	MRI-CGCM3	1.25 × 1.25
20	Norwegian Meteorological Institute, Norway	NorESM1-M	2.5 × 1.875

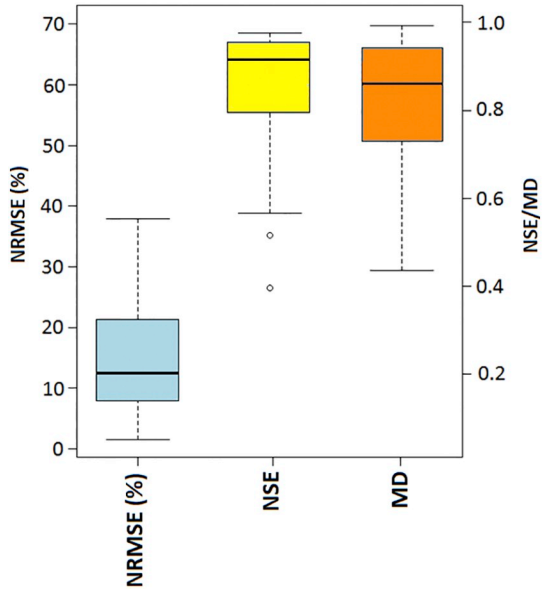

Fig. 3. The performance of GPCC rainfall in replicating observed rainfall of Nigeria in term of three statistical indices.

individual models can be minimized by a careful selection of an ensemble model for climate projection (Knutti et al., 2010; McSweeney et al., 2015). In selecting GCMs that could form a model ensemble, the envelope approach, which involves the assemblage of models with a varying range of projection for one or more climate variables gathered from a pool of available models, has been used (Houle et al., 2012; Immerzeel et al., 2013; Sorg et al., 2014). The past performance involving the ability of the climate model to simulate the past, and the present climate was used by Pierce et al. (2009). Evans et al. (2013) built a sub-ensemble considering the independence of models using unique parameterization which gives the built ensemble similar characteristics as the larger ensembles from which they are assembled. Lutz et al. (2016) applied a combined approach in which model screening was done using the envelope approach after which the past performance approach was used in the selection of the models.

This study selects the most suitable GCMs to form an ensemble GCM for the projection of rainfall in Nigeria. The approach involves the use of feature selection methods using the EG, GR, and SU methods. The selection of the GCMs involves a number of procedures which are given as follows.

1. Resampling/regridding of rainfall data of GCM historical runs to 2° × 2° resolution (30 grid points covering Nigeria), and aggregation of the GPCC data to the same resolution to comply with GCM data.
2. Development of EG, GR and SU models at each grid point using GPCC data as dependent variable and the different GCMs as the independent variables to simulate rainfall for the period of 1961 to 2005.
3. Ranking of GCMs using estimated weights from the EG, GR, and SU models at the various grid points within the study area.
4. Delineation of the GCM ensemble from the aggregation of the ranking patterns at the 30 grids using MCDM.

Details about the methods used in weighing of GCMs and the approach for the ranking and selection of the GCMs using MCDM are discussed as follows.

3.1.1. Entropy gain

Because the loss of information and chaotic evolution in dynamical systems can be measured using information entropy, they become an important tool in the study of the evolution of dynamical processes of physical systems (Ma and Ma, 2018). Based on the concept of theoretical information, EG measures the uncertainty of a random variable (Yu and Liu, 2004). Among non-linear correlation measures, many are based on this concept. For variable S, the information entropy (I) (Karewgowda et al., 2010) is given as:

$$I(S) = -\sum_{i=1}^{m} P_i \log_2(P_i) \quad (1)$$

where P_i is the probability of an arbitrary sample belonging to class Ci and is estimated by s_i/s. Here, s_i is the sample belonging to class Ci and s is the total number of data.

The entropy of a variable is said to be high if it is uniformly distributed (Guyon and Elisseeff, 2003). In contrast, if there is skewness in the distribution, then the data set entropy is low. While still restricted to the same symbol (symbol as variable example here), a sources entropy ratio to the allowable maximum value is its relative entropy (Shannon, 1948). One minus the relative entropy gives the redundancy.

3.1.2. Gain ratio

The concept of the gain ratio (GR) is to rank features based on

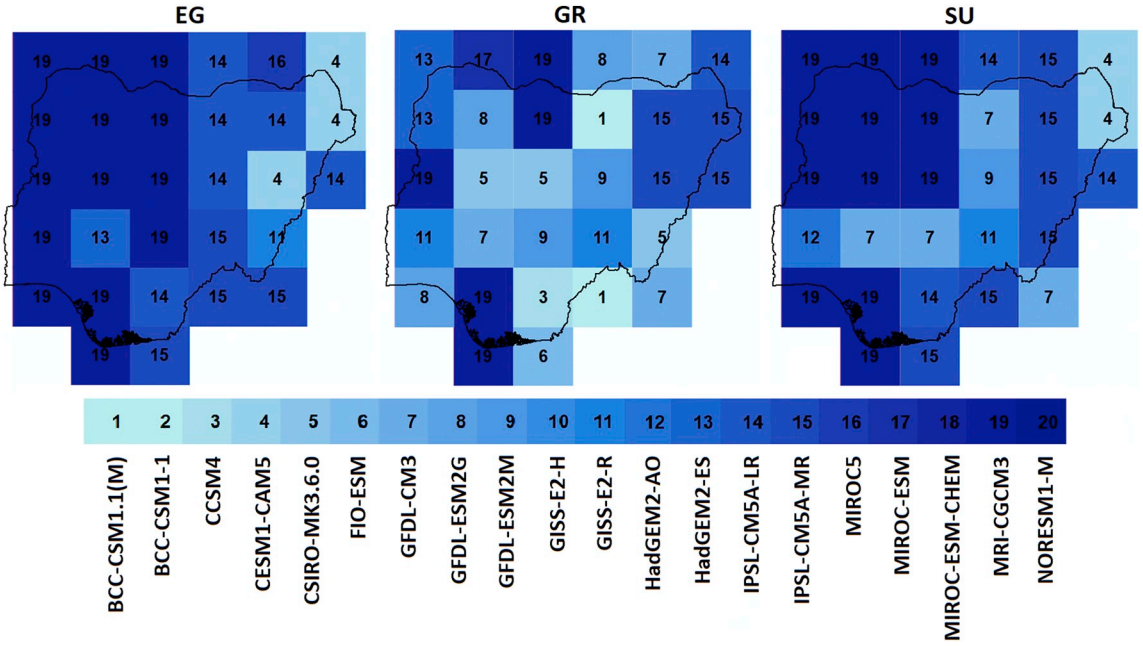

Fig. 4. Spatial distribution of the GCMs ranked top by EG, GR, and SU methods.

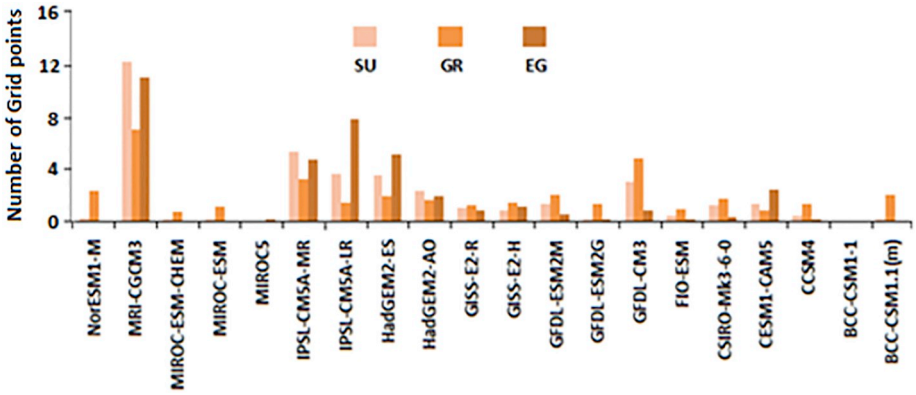

Fig. 5. The number of grid points at which each different GCMs were ranked top by SU, GR, and EG methods.

Table 2
The weights estimated for four selected GCMs by different feature selection methods and rankings of GCMs based on estimated weights.

Models	EG	GR	SU	Rank
MRI-CGCM3	6.09	5.01	6.76	1
HadGEM2-ES	6.35	3.34	5.52	2
CSIRO-Mk3.6.0	4.43	3.56	4.47	3
CESM1-CAM5	4.37	2.83	3.8	4

information entropy. For a set S consisting of s data samples having distinct classes, the expected information that a given sample classification requires is as given in Eq. (1) (Karewgowda et al., 2010).

Letting an attribute A have v distinct values, and S_{ij} be number of samples of class C_i in a subset S_j. the samples in S that have value a_j of A are contained in S_j. On the basis of the partitioning into subsets by A, the expected information (E) is given by:

$$E(A) = -\sum_{i=1}^{m} I(S)\frac{S_{1i} + S_{2i} + \ldots + S_{mi}}{S} \quad (2)$$

By branching on A, the gainful encoding information is given as:

$$G(A) = I(S) - E(A) \quad (3)$$

For a test on the A attribute, the information generated by splitting the training data set S into v partitions corresponding to v outcomes is given by:

$$SP_A(S) = -\sum_{i=1}^{v} (|S_i|/|S|)\log_2(|S_i|/|S|) \quad (4)$$

Gain Ratio is defined as follows:

$$GR(A) = \frac{G(A)}{SP_A(S)} \quad (5)$$

In the GR technique, the attribute with the highest gain ratio is chosen as the splitting attribute. Gain ratio has the ability to correct non-justifiable favoritism of information gain and the creation of an unbalanced tree where large variance exists between leaves depths (Harris-J, 2001).

3.1.3. Symmetrical uncertainty

Based on the theoretical concept of information entropy, the symmetrical uncertainty (SU) assesses the features influence on outcomes and can be used in feature classification from the evaluation of the features goodness (Jiang et al., 2008). The steps involved in SU's feature selection approach follows those of Eqs. (1) and (2). This is followed by the information gain given in Eq. (3). Lastly, dividing the information gain (IG) by the entropy sum of outcome and feature variables in

Table 3
Results of performance metrics of four bias correction methods.

	NRMSE	PBIAS	NSE	RSD	MD		NRMSE	PBIAS	NSE	RSD	MD
	CESM1-CAM5						HadGEM2-ES				
SCL	38.5	0	0.85	0.99	0.84	SCL	34.6	0	0.88	1	0.86
GEQM	100.2	−100	−0.01	0	0.66	GEQM	100	−100	0	0	0.67
PT	53.2	0	0.72	1.04	0.76	PT	0	0	0.73	1.04	0.77
GAQM	45.8	0.4	0.79	0.97	0.82	GAQM	44.7	1.2	0.8	0.97	0.82
GCM	79.6	−18.1	0.36	1.14	0.68	GCM	42.9	−7	0.82	1.06	0.83
	CSIRO-Mk3.6.0						MRI-CGCM3				
SCL	44	0	0.81	0.95	0.82	SCL	30.7	0	0.91	1.01	0.88
GEQM	100	−100	0	0	0.66	GEQM	100	−100	0	0	0.66
PT	47.5	0	0.77	1.06	0.79	PT	48.8	0	0.76	1.06	0.78
GAQM	40.6	0.8	0.83	0.98	0.84	GAQM	41.1	4.3	0.83	0.95	0.83
GCM	82.1	−42.9	0.33	0.65	0.65	GCM	59	23	0.65	1.2	0.8

SCL: Scaling; GEQM: General Quantile mapping; PT: Power transform; GAQM: Gamma quantile mapping; GCM: General circulation model.

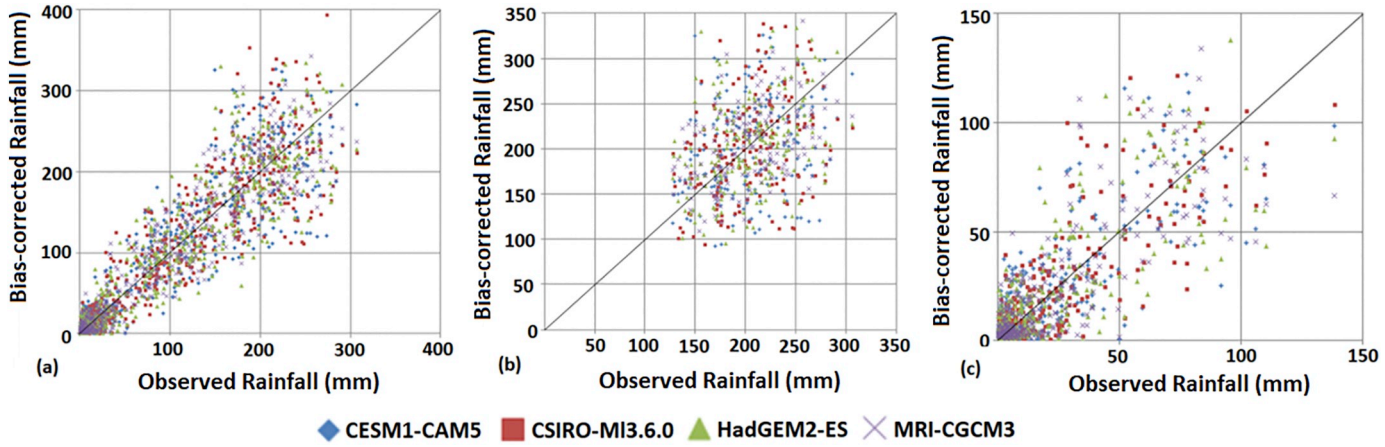

Fig. 6. Scatter plots showing the relationships between the downscaled and the GPCC monthly rainfall for the (a) year round, (b) rainy season, and (c) dry season.

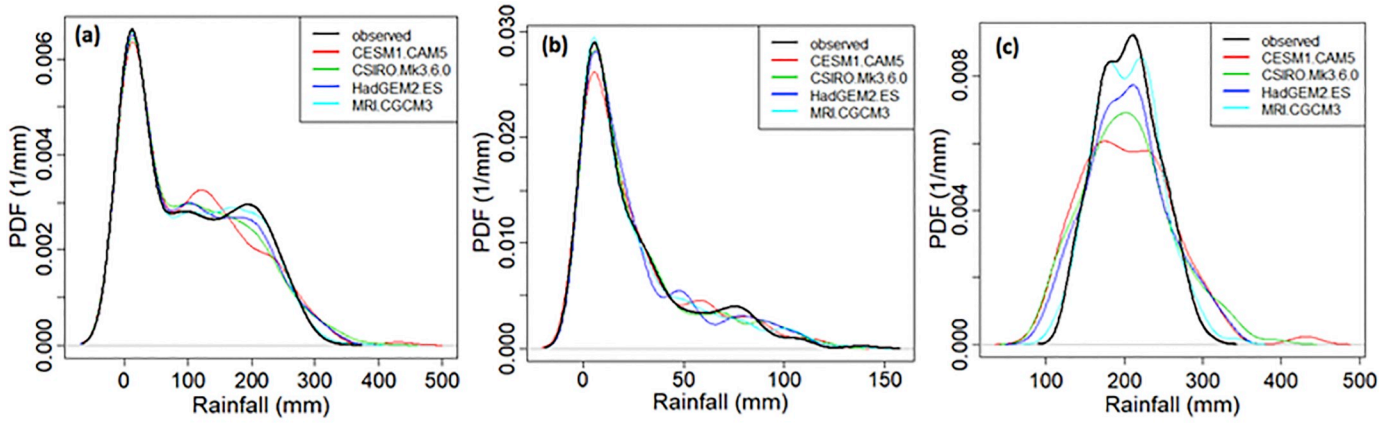

Fig. 7. PDF curves of downscaled and GPCC monthly rainfall for the (a) year round, (b) rainy season, and (c) dry season.

compensation for the bias of the IG in favor of the features with more values gives the estimated SU:

$$SU(X_i, Y_j) = \left[\frac{2IG(X_i \mid Y_j)}{H(X_i) + H(Y_j)}\right] \quad (6)$$

where $IG(Y_j)$ is the information gain between features, X_i and Y_j, and $H(X_i)$ and $H(Y_j)$ represent the entropies of X_i and Y_j, respectively. SU values range from 0 and 1, and the feature having the larger SU values is given the higher weight.

3.1.4. GCMs ranking using multi-criteria decision making

In decision analysis, the provision of the exact fundamental values for alternative evaluation is arduous (Vetschera et al., 2014). This is also the case at a more detailed level when underlying preference model like weights assignable to different attributes for some parameters are considered. Multi-criteria decision making (MCDM) methods for information combination from various sources by aggregation can be an efficient tool in ranking many alternatives. This study therefore employed MCDM whereby GCMs are ranked on the basis of their weights generated using the earlier discussed feature selection methods. The approach involves the use of a payoff matrix in which the number of grid points for which a model achieves a certain rank from the total number of grid points within the study area is seen in the matrix. This study uses 20 GCMs; therefore the dimension of the payoff matrix is

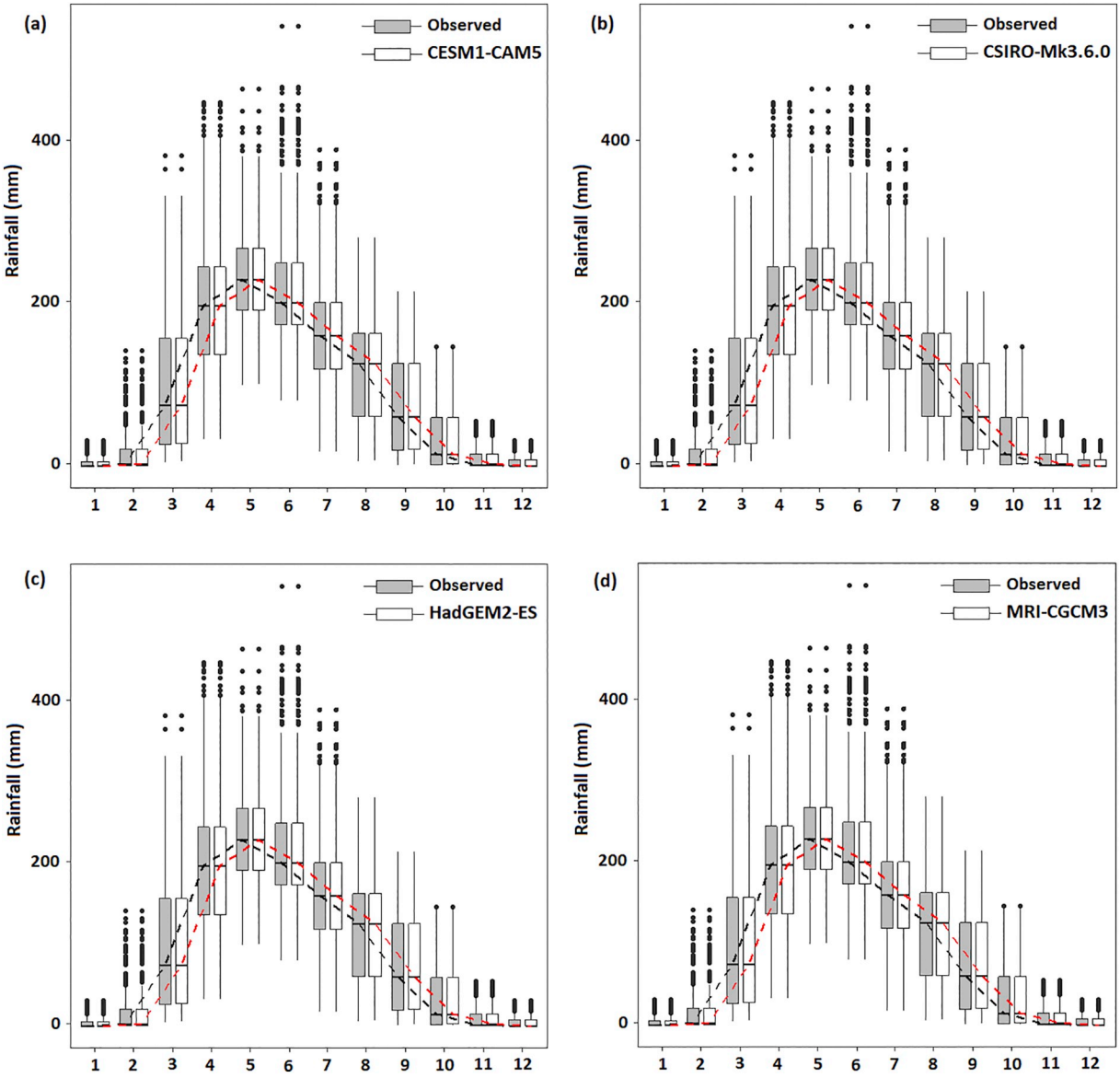

Fig. 8. Boxplots of the GPCC and downscaled monthly rainfall of different GCMs. The X-axis represents different months of a year.

20 × 20 i.e. ranking ranging from 1 to 20. The performance of a model is quantified from its frequency of occurrence from the total grid points within the study area. Also, a higher frequency of occurrence for a model corresponds to a higher weight, and hence that model has a higher ranking.

3.2. Bias correction of GCMs

Bias correction involves the correcting of biases through feeding of regional climatic information into GCMs (Akhter et al., 2017). There are different types of bias correction methods including: the delta change method (Hay et al., 2000), multiple linear regression (Hay and Clark, 2003), local intensity scaling (Schmidli et al., 2006), monthly mean correction (Fowler and Kilsby, 2007), gamma-gamma transformation (Sharma et al., 2007), analog methods (Moron et al., 2008), fitted histogram equalization (Piani et al., 2010), quantile mapping (Wood et al., 2004; Sun et al., 2011), and the scaling method (Mahmood and Jia, 2017). Among these methods, the scaling, quantile mapping and power transform have been widely used because of their simplicity but better correction capability.

Therefore, this study uses linear scaling, gamma quantile mapping, power transform, and general quantile mapping to correct the biases from the historical (1961–2005) GCM rainfall in respect of GPCC rainfall. Standard statistical indices; percentage of bias (Pbias), normalized root mean square error (NRMSE), Nash-Sutcliff efficiency (NSE), modified index of agreement (MD) and relative standard deviation (RSD) were used in assessing the performances of the models. The highest performing bias correction method was then selected for the downscaling of the future rainfall of Nigeria.

3.3. Ensemble projections

The regression-based MME has the ability of preserving the variance in the average of the MME and has been widely adopted in recent times. However, multiple linear regressions lacks the ability to explicate the nonlinear relationship between the independent and the dependent variables, even when there is significance in their relationship. RF can however explain the regression coefficient (Li et al., 2011) and has therefore been used in converting the selected rainfall GCMs into a single ensemble in this study. RF is a non-parametric statistical regression algorithm that produces numerous independent regression and classification trees (CART).

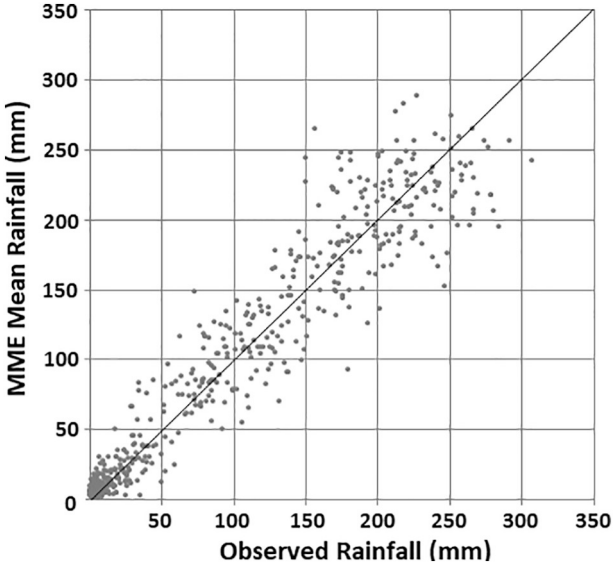

Fig. 9. Scatter plot of RF estimated MME mean monthly rainfall and GPCC mean monthly rainfall averaged over Nigeria for the period 1971–2005.

RF has been identified as an effective and robust algorithm of generation of MME in this study because: (1) the robustness of RF may avoid over-fitting; (2) many different types of input variables can be implemented without variable deletion and regularization; and (3) it has an analytical and operational flexibility. Thus, it is expected that RF would be useful to build regression models for precipitation in relation to a number of predictors across different spatial scales.

The spatial and temporal variations of rainfall over Nigeria estimated from the average variances of MME rainfall were projected for the periods 2010–2039, 2040–2069, and 2070–2099, and analyzed against the historical period of 1971–2000.

3.4. Quantile regression

The QR works similar to ordinary linear regression method but in QR the regression coefficients are quantile-dependent. For example, a linear regression equation $y_q = a_q + b_q x + \varepsilon_q$ can be considered as QR if q is quantile (values between 0 and 1). The regression coefficients, a_q and b_q depend on the value of q which can be estimated to minimize the objective function as follows:

$$Q = \sum_{i:y_i \geq a_q + b_q x_i} q\ |y_i - a_q - b_q x_i| + \sum_{i:y_i < a_q + b_q x_i} (1-q)|y_i - a_q - b_q x_i| \quad (7)$$

where y denotes the rainfall and x is the year of record.

4. Results

4.1. Performance assessment of GPCC rainfall

The assessment of the ability of GPCC rainfall data in replicating the properties of the observed rainfall data of an area is crucial as the outcome of any study using gridded data can be affected by their reliability. In the present study long-term monthly rainfall data available at 37 locations of Nigeria with different time spans were used to validate the performance of GPCC rainfall data. The rainfall time series of a station was compared with the rainfall time series of the nearest GPCC grid point (Ahmed et al., 2019; Nashwan et al., 2019) using three statistical indices namely, NRMSE, NSE and MD. Obtained results are presented using box plots in Fig. 3. The results showed that mean NRMSE, NSE and MD values for rainfall was 11.8%, 0.79 and 0.82 respectively for all the stations. The NSE and MD were found near to 1 at many stations. The results indicate the ability GPCC rainfall to be used for climatic study in Nigeria.

4.2. Selection of GCM ensemble

The spatial ranking for the 20 rainfall GCMs used in this study by the three feature selection methods are presented in Fig. 4. The models shown are the ones that ranked the highest among all the 20 GCMs. The rankings of MRI-CGCM3 model are higher in the SU and EG methods. The model IPSL-CM5A-MR also shows high ranking for the three methods, and the model IPSL-CM5A-LR for the EG method. Other models that rank high are CSIRO-MK3.6.0, GISS-E2-R, GFDL-ESM-2 M for the GR method, CESM1-CAM5 for the EG and SU methods, and GFDL-CM3 for the SU and GR methods.

The number of grid points at which each of the 20 GCMs achieved top rank for EG, GR and SU methods are summarized in Fig. 5. As seen, the MRI-CGCM has overall the highest weight for all the methods. This is followed by the models, IPSL-CM5A-MR, HadGEM2-ES, IPSL-CM5A-LR, HadGEM2-AO, CESM1-CAM5, and GFDL-CM3.

A MCDM which combines information from different feature selection methods was used to rank the GCMs. A payoff matrix whereby the matrix shows the number of grid points for which a model achieved a certain rank from the total number of grid points was generated for each feature selection method. The payoff matrix was used for estimation of weights for different GCMs. The weights estimate for four selected GCMs by each of the feature selection methods are shown in Table 2. MRI-CGCM3 ranked the 1st for GR and SU, and 2nd for EG, the model HadGEM2-ES ranked 1st for EG, 2nd for SU, and 3rd for GR, CSIRO-Mk3–6-0 ranked 2nd for GR, and 3rd for EG and SU while CESM1-CAM5 ranked 4th for all the methods. Final rankings were assigned to each of the models based on their ranking from each of the feature selection methods.

4.3. Performances assessment of bias correction methods

The individual averages of monthly rainfall for the four selected models were compared to that of the GPCC in order to assess the performance of the downscaled models. The performances of the four bias correction methods, linear scaling (SCL), gamma quantile mapping (GAQM), power transform (PT), and general quantile mapping (GEQM) are presented in Table 3 by five indices. The performance of raw GCM in simulating GPCC rainfall is also provided in the table to compare the improvement obtained after bias correction. Aside from the model CSIRO-Mk3.6.0 for which GAQM shows better performance than the SCL, the SCL shows the overall highest performance for the individual models. The SCL was therefore chosen for the downscaling of the selected models to form an MME model for Nigeria.

4.4. Performance evaluation of downscaling models

The scatter and probability distribution function (PDF) plots were used to assess performances of downscaling models based on SCL. The performance was assessed for all the four selected GCMs in comparison to GPCC rainfall for the dry and rainy seasons and for the year round.

The average monthly rainfalls for the four selected models compared to that of the GPCC for the year round, rainy season, and the dry season in scatter plots are presented in Fig. 6. It can be seen that the estimates of the downscaled models are close to those of the GPCC. Thus, SCL for bias correction is very efficient in the downscaling of the GCMs.

The PDFs of the downscaled models have been compared to those of the GPCC rainfall in order to check their ability in replicating the average, variance, and distribution of rainfall of that of the GPCC. The PDFs for the GPCC and the downscaled models are presented in Fig. 7. Both are closely matching especially for the year round and the rainy seasons. This is indicative of the ability of SCL to correct the biases in

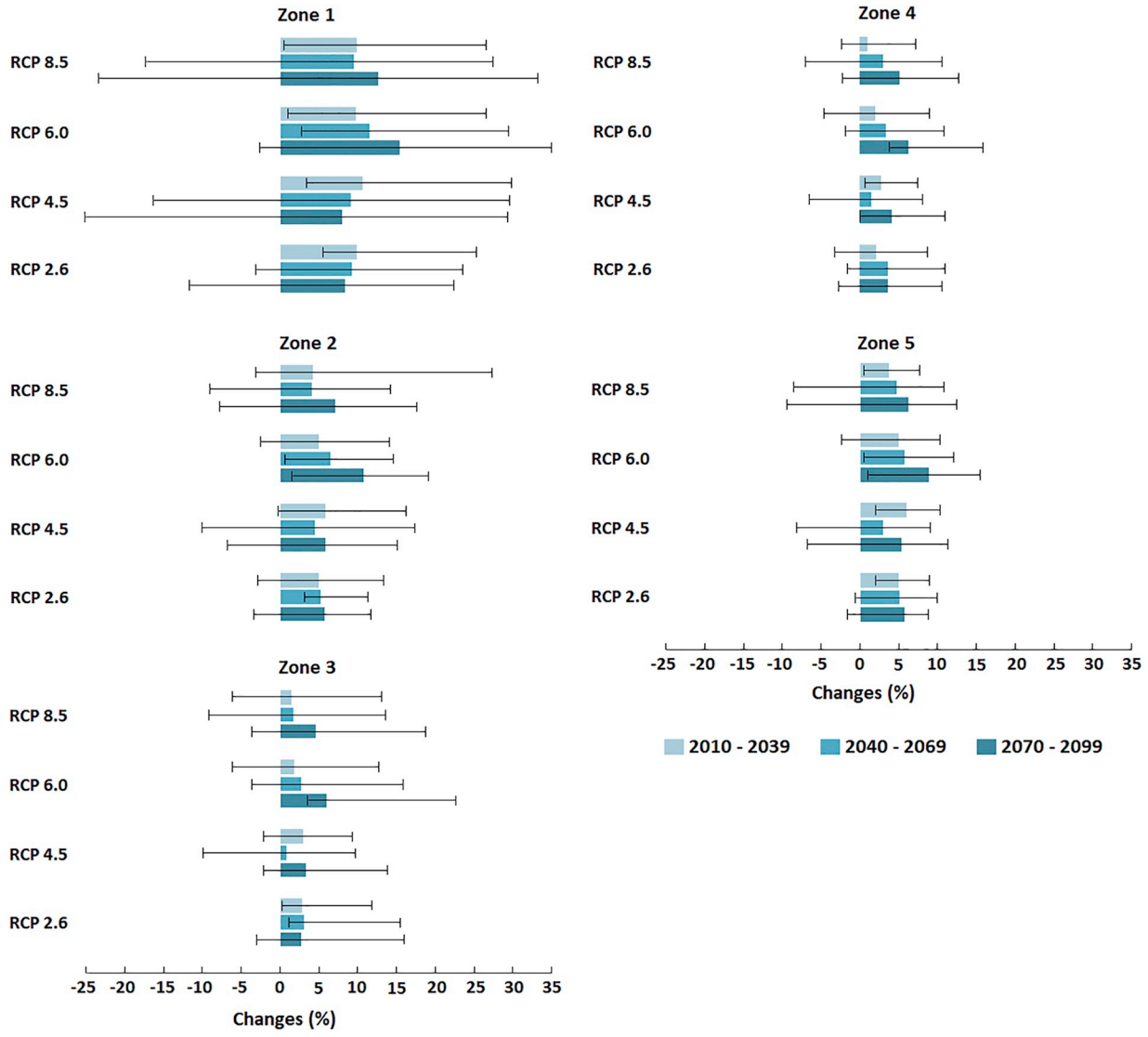

Fig. 10. Changes (%) of annual average precipitation with 95% level of confidence at different ecological zones of Nigeria during three future periods and for all RCP scenarios.

the GCMs.

The performances of SCL in downscaling the four selected GCMs were assessed using boxplots. Box plots of the monthly averages of GPCC are compared to those of the downscaled models estimated for the 323 grid points for the four selected GCMs as shown in Fig. 8. The figure shows complete matching of the mean, quartiles and range of downscaled rainfall with the GPCC rainfall. Therefore, it can be concluded that SCL showed good performance in downscaling the GCMs.

4.5. Rainfall projection

This section presents the results of the projections from the ensemble downscaling model. The projections were considered for RCP 2.6, RCP 4.5, RCP 6.0, and RCP 8.5. So, the RCPs were separately downscaled for the 323 grid points within the study area. RF regression was used in the computation of the MME of projected rainfall at all grid points for each RCP. The obtained results from the MME means of rainfall projections are presented as follows.

4.5.1. Multi-model ensemble mean of rainfall

The scatter plots of the MME mean rainfall and that of the GPCC averaged for the 323 grid points for the historical period 1971–2005 is presented in Fig. 9. As it is seen, there is a close relationship between the estimated MME and the GPCC mean rainfall. It indicates the great performance of the RF in the MME computation. For each grid point, the correlation coefficients between the observed and the estimated MME fall at least to a value of 0.94. It can therefore be concluded that the estimated MME using RF can improve the accuracy in projection as the associated uncertainties with the individual GCMs can be reduced. MME mean was estimated using the RF regression model at a 95% confidence interval to show projection uncertainties.

4.5.2. Changes in annual rainfall

The percentage changes in annual rainfall projected for all RCPs were compared to the base rainfall (GPCC) (1971–2000) for the different ecological zones (Fig. 1) are presented in Fig. 10. To estimate rainfall changes, the average of the GPCC rainfall for the period 1971–2000 at all grid points were subtracted from those of the projected rainfalls for the different future periods, 2010–2039, 2040–2069, and 2070–2099. The future changes in rainfall and the levels of uncertainty were estimated using the MME mean and its 95% confidence band. There is variation in rainfall changes projections from zone to zone, and from period to period for the different RCPs. The arid and semi-arid regions of the north where rainfalls are normally low in the

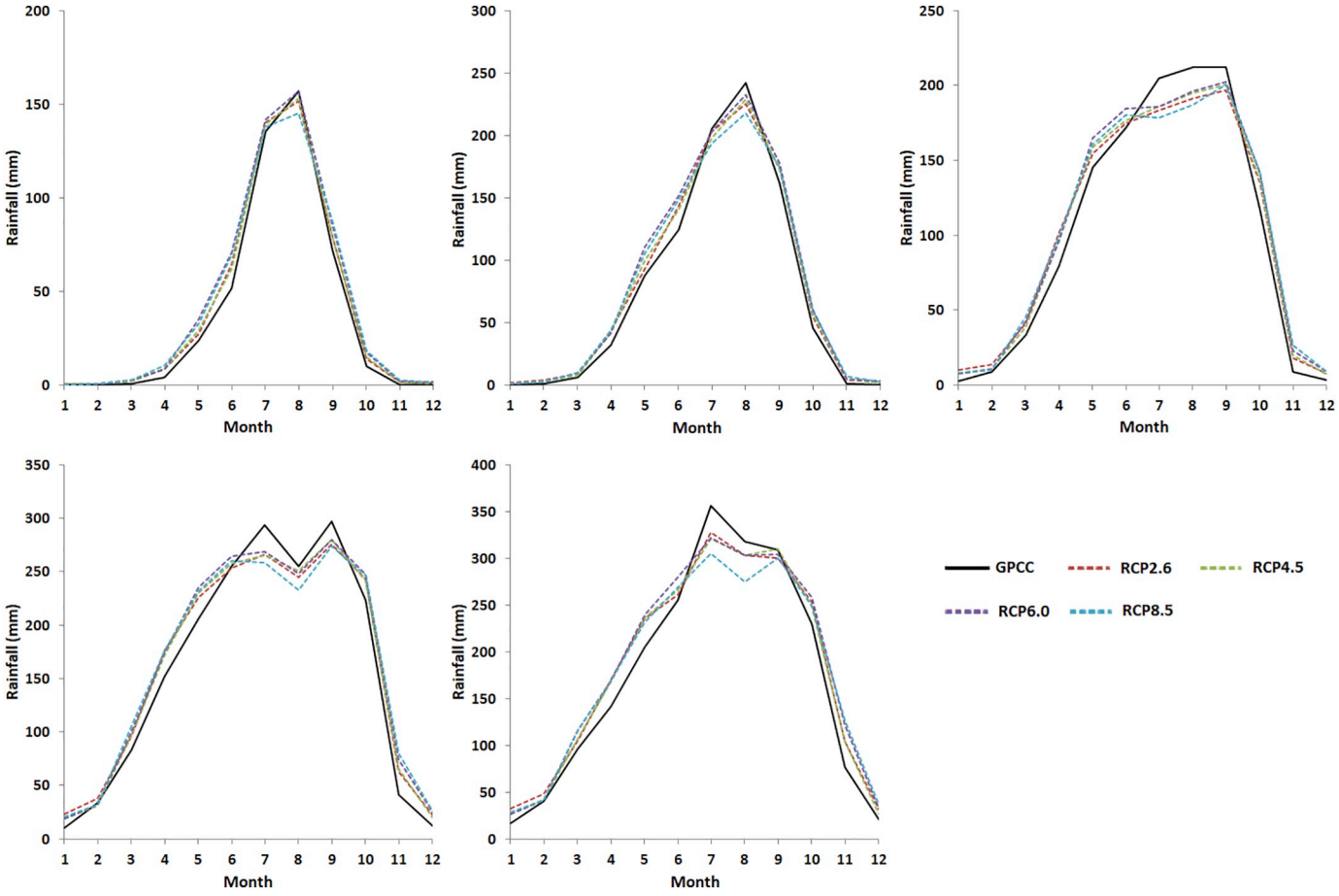

Fig. 11. Projected changes (%) in monthly rainfall in different regions of Nigeria between 2070 and 2099.

Sahel savanna (zone 1) are generally projected to have the highest percentages of changes in rainfall for all RCPs and for all future periods. This is followed by the Sudan Savanna (zone 2) also in the north, and the mangrove swamp (zone 5) in the south. The Guinea savanna (zone 3) and the rainforest (zone 4) showed the lowest percentage changes in rainfall. Rainfall changes which increased for all periods and for all RCPs ranges between 1% and 10.5% for the period, 2010–2039, 0.7% and 11.4% for the period, 2040–2069, and 2.4% and 15.2% for the period, 2070–2099.

The highest levels of uncertainties were found in RCPs 4.5 and 8.5 for the periods, 2070–2099 and 2040–2069 at the arid northern part. Uncertainties are also generally high in this zone compared to the other zones, and is supported by other studies which confirmed that uncertainties in water availability are higher in arid areas (Scherer and Pfister, 2016). Uncertainties are lowest at the southern mangrove swamp where the rainfalls are the highest in the country. The uncertainties across the zones showed inconsistency indicating that rainfall changes can both increase and decrease.

4.5.3. Changes in seasonal rainfall

Seasonal changes of rainfall for the period 2070–2099 were assessed for the different zones in Nigeria by averaging the monthly rainfalls for all grid points as presented in Fig. 11. At zone 1, the changes in rainfall during this period will be higher than those of GPCC for all RCPs. However, the RCPs 2.6, 4.5, and 8.5 shows lower changes in rainfall between July and August. At zone 2, while rainfall increments are observed for most of the rainy months, changes in rainfall decreased between July and August for all RCPs. Similarly, changes in rainfall decreased from middle June to the end of September at zone 3 for all RCPs. Other rainy periods for this zone show higher increases in projected rainfalls for all RCPs. At zones 4 and 5, the period between June and September also shows that rainfalls are decreasing for the projections for all the RCPs. Other periods however show increases in rainfall projections. The rainfalls are decreasing highest at the zones 3, 4, and 5 where the rainfalls are usually high. Decreases in rainfall for this period are highest for RCP 8.5 at all zones and especially at zone 5. The highest increases in rainfall are observed between April and June in zones 4 and 5, while increases are occurring in the semi-arid zones 1 and 2 during the month of June when the rainfalls are just starting. Other months after the peak of rainfalls, occurring between August and September in the north and during July and August in the south shows slight increases in the projected rainfalls.

4.5.4. Spatial changes in annual rainfall

Spatial rainfall change distributions can be of significance in enabling the better understanding of the future rainfall variations at different locations. The distribution of the changes in annual rainfall over Nigeria for the future projections 2010–2039, 2040–2069, and 2070–2099 were spatially mapped for all RCPs as shown in Fig. 12. It is important to mention that the description of the different parts of the study area is not based on the geopolitical zones commonly used in Nigeria, but on equidistance from the north to the south, and from the west to the east.

The maps show increases in some parts of the country for all RCPs and for the considered periods, while significant decreases are also observed at other locations. For the period 2010–2039, increases in rainfall occurred at many locations with the highest increases observed at the north eastern part for all RCPs and also at parts of north western and parts of south western Nigeria for RCP 6.0. Decreases in rainfall for this period are observed at the north western and the south eastern

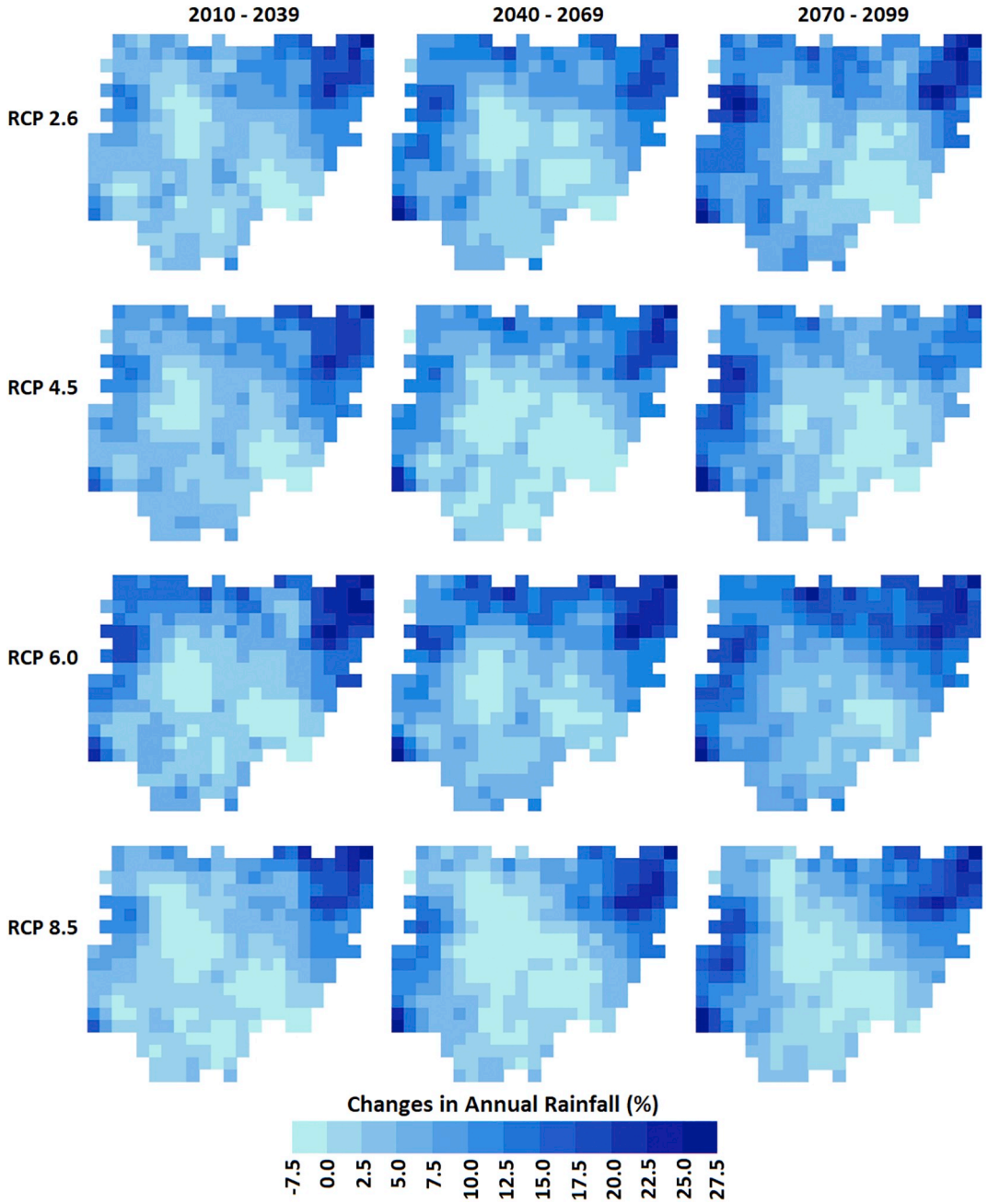

Fig. 12. Spatial distribution of annual average rainfall for 4 RCPs for the three future periods.

parts for all RCPs and, additionally at the south western and south southern parts for RCPs 2.6, 6.0 and 8.5. Projections between the periods 2040–2069 show increases in rainfall for most parts of the north for all RCPs. However, infringing decreases occur at the north western parts for all RCPs and especially for RCP 8.5. Other parts showing rainfall decreases are the central parts which are very extensive for RCPs 4.5 and 8.5. Decreases are also occurring at the south eastern parts for all RCPs and at the south southern parts for RCPs 4.5 and 8.5. The period 2070–2099 shows the highest increases in rainfall. Increases in rainfall are seen in most parts of the north except for some parts in the north east and central for RCPs 2.6 and 4.5, and some parts in the north west and central for RCP 8.5. In the south, rainfalls are decreasing at the south eastern parts for this period. The highest increases in rainfall are observed for the RCP 6.0 for all the future projections, while the highest decreases occurred for RCP 8.5 for the same periods.

4.5.5. Spatial changes in seasonal rainfall

The spatial patterns of the percentage changes in rainfall for the rainy season are presented in Fig. 13. It shows the rainfall increased for all RCPs in most of the northern parts which are known to have lesser amounts of rainfall. However, in the north west, some few locations showed decreases in rainfall ranging between −5% and − 20% for RCP 8.5 during the period 2040–2069.

Increases in rainfall percentages are highest at the north eastern part. In the south, rainfalls are generally decreasing with the highest decreases occurring at the south eastern parts. However, some parts of the south west shows increases in rainfall occurring the highest for all RCPs for the period 2070–2099, RCP 2.6 for the period 2040–2069, and RCP 4.5 for the period 2010–2039.

The spatial pattern of the percentage changes in rainfall for the dry season is presented in Fig. 14. Though rainfalls are generally low for this season averaging a maximum of 60 mm for the four months

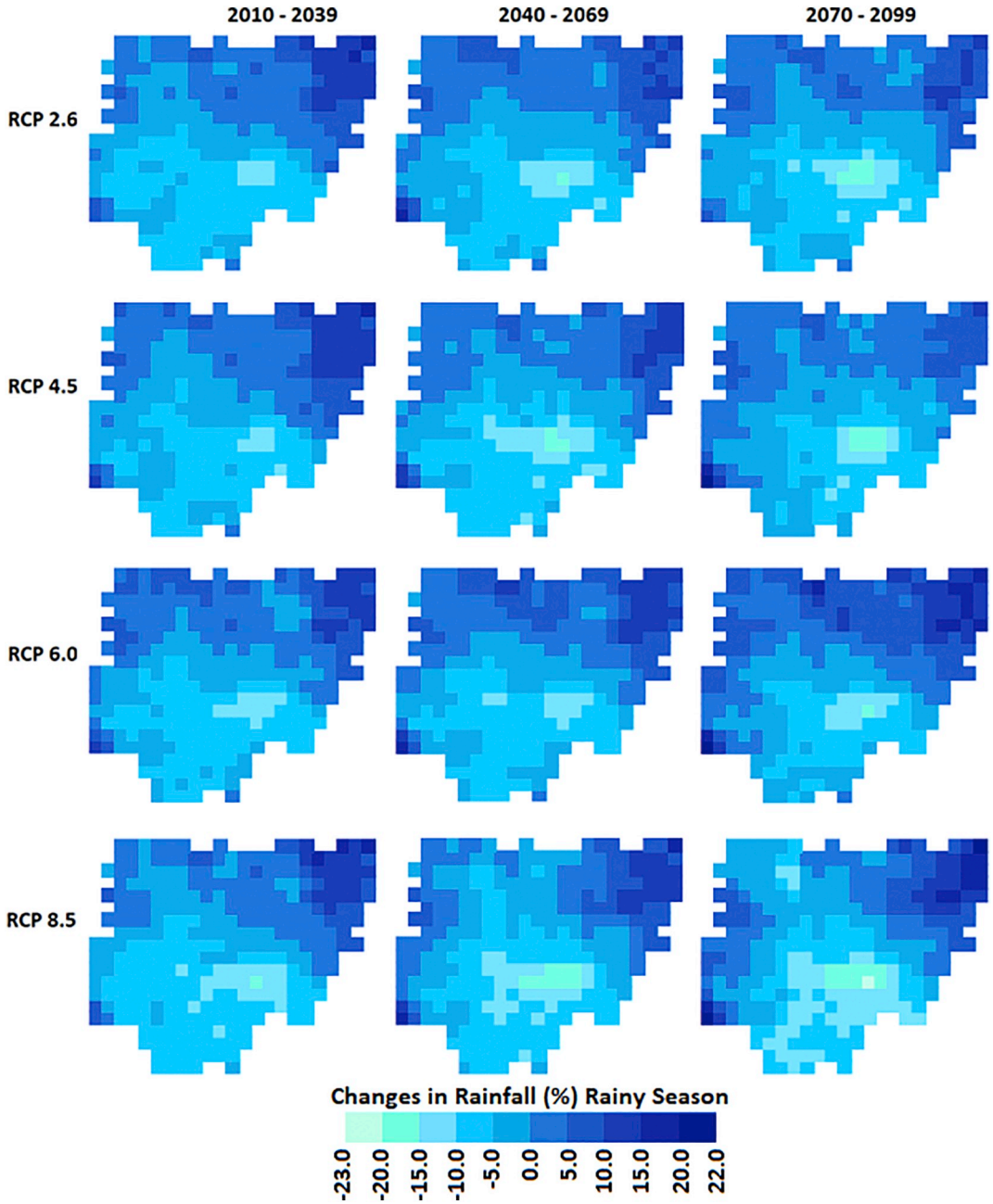

Fig. 13. Spatial distribution of average rainfall for rainy season for 4 RCPs for the three future periods.

between December and March, the higher percentages of increases in rainfall are observed for this season compared to the rainy season. Similar to the rainy season and annual analysis, the highest increases are also seen at the northern arid regions. Few grids are however found to have decreases in the percentage change in rainfall in this region. In the southern part, rainfall increased between 0 and 80% for all RCPs. The least increases occur at the south western parts for most of the RCPs.

4.5.6. Changes in seasonal rainfall with confidence interval

Increases in high and low rainfalls at 95% confidence level were assessed using QR at 2.5% and 97.5% values of projected monthly average of the dry season and the rainy season rainfalls of Nigeria. This was conducted for the five ecological zones as shown in Fig. 15. Increases in maximum and minimum rainfalls vary from the north to the south with more variability observed at the southern parts. At all the zones except zone 4 during the rainy season, there are decreases in the maximum changes in rainfall of RCP 8.5 till the end of the century. However, the minimum increases are seen at zone 2 and zone 3 for this RCP. While other RCPs did show much increases in the minimum increasing rainfall, RCP 6.0 shows a high increase in rainfall up till the end of the century at zone 5. During the dry season, changes in rainfall are lower with the least changes observed at the northern Sahel and Sudan areas and the highest increases at the mangrove swamp area of the south. An increasing trend is observed for the maximum increases in rainfall overtime for all RCPs except for RCP 4.5. The highest increases are observed for RCP 2.6 during this season.

5. Discussion and conclusions

A scaling bias correction method has been used in this study for the downscaling of selected rainfall GCMs to create a model ensemble for climate projections for Nigeria. Four GCMs were selected using the

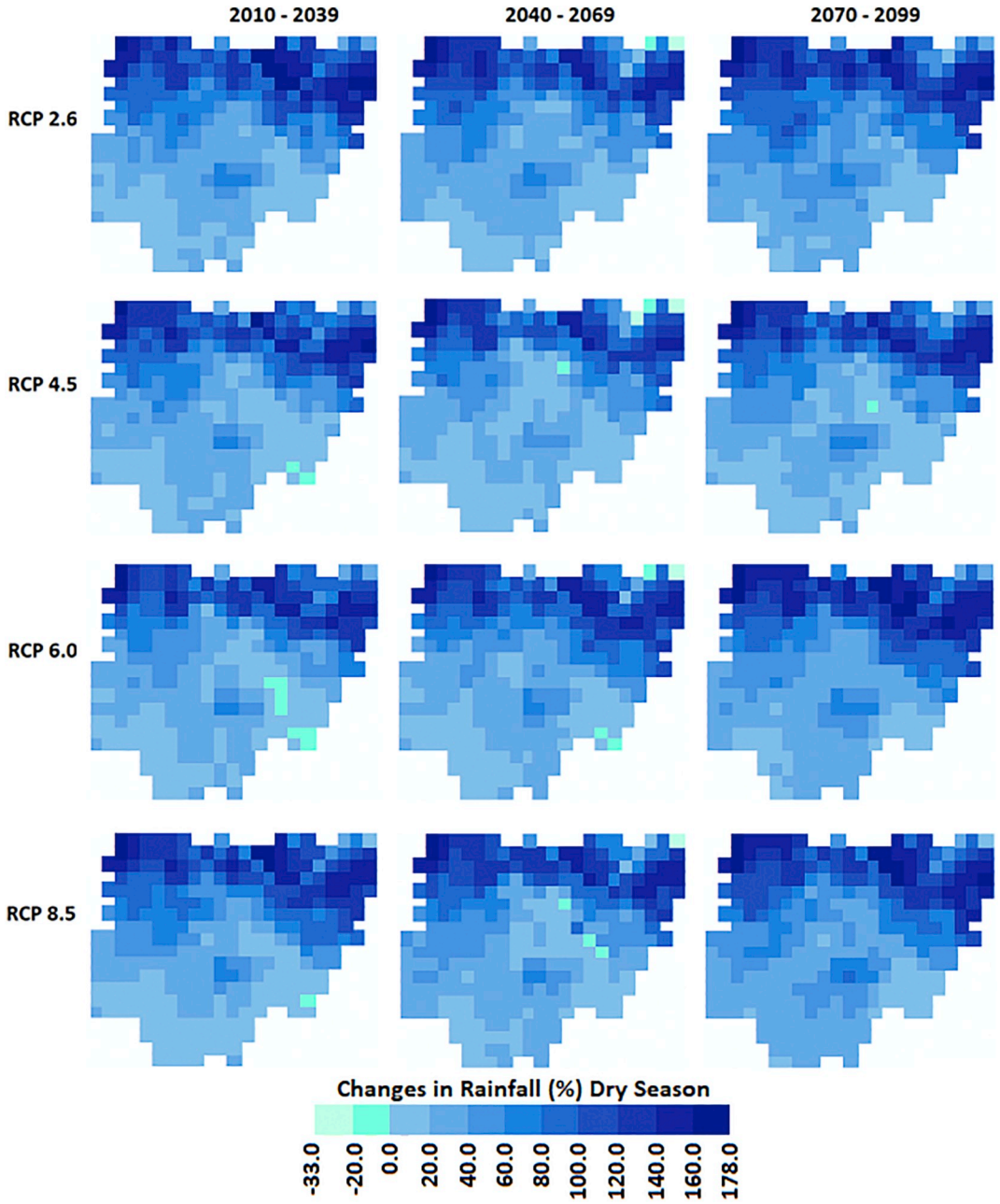

Fig. 14. Spatial distribution of average rainfall for rainy season for 4 RCPs for the three future periods.

feature selection methods SU, EG, and GR, and a MCDM from a total of 20 GCMs of the CMIP5. The selected models were downscaled using scaling bias correction method, and the model performance was evaluated with the reference GPCC rainfall data using various approaches. The performance assessment showed that the SCL is efficient in correcting the individual biases existing in all GCMs. The MME average was estimated from the downscaled models using RF and its 95% confidence interval for rainfall projections with estimations of the uncertainty levels.

The study revealed that annual average rainfall increased at various ranges across most grid points within the study area for all RCPs and for all future periods. However, rainfall increases are highest for all periods for all RCPs at the arid and semi-arid regions where rainfalls are the lowest and, at the south western parts for all RCPs during 2040–2069 and 2070–2099. Thus, a general pattern being observed is that dry regions are getting wetter. This contrasts the findings of Liu and Alan (2013) at the global scale, which has already been refuted previously (Greve et al., 2014). The number of grid points for which rainfalls are decreasing for the projected periods also varies for the RCPs. RCPs 2.6 and 4.5 for the period 2010–2039, and RCP6.0 for the period 2070–2099 showed the least number of grid points for which rainfalls are decreasing. In contrast, the highest number of grid points for which there were decreases in rainfall are observed for all other RCPs with the highest being RCP 4.5 for 2040–2069 period and RCP 8.5 for all the periods.

Seasonal percentage changes in rainfall show that rainfalls will increase between the range of 0–20% in most parts of the north especially in the north east with some decrease in rainfall at few locations in the north west during the rainy season. The southern parts where rainfalls used to be high will experience a general decrease in rainfall with the highest decreases occurring in the south eastern parts particularly in Benue state (Fig. 1), known for its extensive agricultural practices and therefore termed “the food basket of the nation”. Atedhor (2016) reported delayed rainfall onset in the Benue area resulting in the

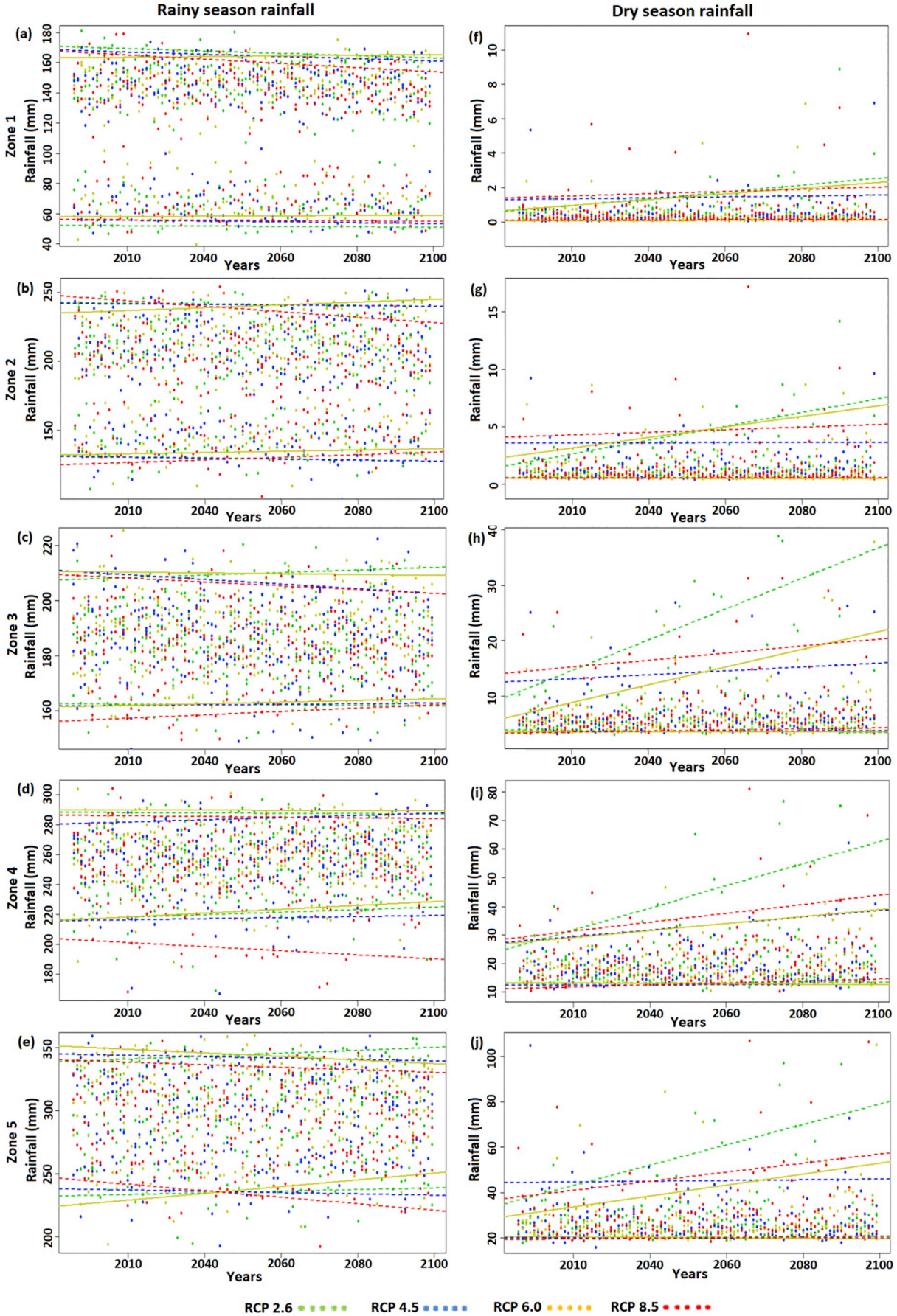

Fig. 15. Projection of monthly mean of dry season (14a–14e) and rainy season (14f–14j) rainfall with 95% confidence band for all the five climatic zones of Nigeria.

constriction of the growing seasons, and a negative deviation from normal in precipitation to up to 35% in some growing season months. This indicates a drying trend in the area and less availability of rainfall during growing seasons. The Benue area and the surrounding Kogi and Nassarawa states (Fig. 1) among some other states have been experiencing more frequent violent clashes between farmers and herders due to resource competitions for which climate change has been attributed to be one of the major causes (Merietu and Olarewaju, 2009; Weezel, 2017; Okoli and Atelhe, 2014; Ubelejit, 2016). In the dry season, the percentages of increase and decrease in rainfall are highest compared to the annual and the rainy season period. However, decreases in percentages of rainfall are at just few grid points across the country. Increases in rainfall almost doubled at some areas reaching up to 178% in the arid northern parts. In the south, percentage increases in rainfall are lower compared to the north occurring within the range of 0–80%.

The changing percentages in rainfall for the future show the importance of this study for Nigeria. This is especially crucial for areas prone to clashes between farmers and herders due to completion for water and grazing lands. It has been unraveled that the increases or decreases in rainfall may increase the risks of flood at some parts and that of droughts at others respectively. With this understanding, the areas that may be more vulnerable to the impacts of the changing climate in the future are identified. This can be significant for planning of appropriate mitigation and adaptation measures towards combating or alleviating the impacts of these changes. Among these are climate-smart agriculture, and rainwater harvesting which might be suitable techniques for Nigeria's rain fed agriculture in areas where rainfall decreases (Scherer and Verburg, 2017). As temperature plays a significant role in disaster risks, a similar study on projected changes in this variable for the same period, for all RCPs will be invaluable in assessing the joint impacts of these variables on disaster risks. It is therefore anticipated that such study be conducted for comprehensive understanding of the joint impacts of the changing climate variables.

Acknowledgements

This study was supported by a grant (NRF-2016R1D1A1B04931844) from the National Research Foundation of Korea.

References

Ahmed, K., Shahid, S., bin Harun, S., Ismail, T., Nawaz, N., Shamsudin, S., 2015. Assessment of groundwater potential zones in an arid region based on catastrophe theory. Earth Sci. Inform. 8 (3), 539–549.

Ahmed, K., Shahid, S., Chung, E.-S., Ismail, T., Wang, X.-J., 2017a. Spatial distribution of secular trends in annual and seasonal precipitation over Pakistan. Clim. Res. 74, 95–107. https://doi.org/10.3354/cr01489.

Ahmed, K., Shahid, S., Othman, R., bin Harun, S., Wang, X.J., 2017b. Evaluation of the performance of gridded precipitation products over Balochistan Province, Pakistan. Desalin. Water Treat. 79, 73–86.

Ahmed, K., Shahid, S., Nawaz, N., 2018a. Impacts of climate variability and change on seasonal drought characteristics of Pakistan. Atmos. Res. 214, 364–374.

Ahmed, K., Shahid, S., Nawaz, N., Khan, N., 2018b. Modelling climate change impacts on precipitation in arid regions of Pakistan: a non-local model output statistics downscaling approach. Theor. Appl. Climatol. 1–18.

Ahmed, K., Shahid, S., Wang, X., Nawaz, N., Khan, N., 2019. Evaluation of gridded precipitation datasets over arid regions of Pakistan. Water 11, 210.

Akhter, J., Das, L., Deb, A., 2017. CMIP5 ensemble-based spatial rainfall projection over homogeneous zones of India. Clim. Dyn. 49, 1885–1916. https://doi.org/10.1007/s00382-016-3409-8.

Atedhor, G.O (2016) Growing season rainfall trends, alterations and drought intensities in the Guinea Savanna belt of Nigeria: implications on agriculture. J. Environ. Earth Sci. Vol.6, No.3, 13Pp.

Becker, A., Finger, P., Meyer-Christoffer, A., Rudolf, B., Schamm, K., Schneider, U., Ziese, M., 2013. A description of the global land-surface precipitation data products of the Global Precipitation Climatology Centre with sample applications including centennial (trend) analysis from 1901-present. Earth Syst. Sci. Data 5 (1), 71.

Ben Daoud, A., Sauquet, E., Bontron, G., Obled, C., Lang, M., 2016. Daily quantitative precipitation forecasts based on the analogue method: improvements and application to a French large river basin. Atmos. Res. 169 (Part A), 147–159. https://doi.org/10.1016/j.atmosres.2015.09.015.

Breiman, L., 2001. Random forest. Machine Learning 45 (1), 5–32.

Douglas, I., Alam, K., Maghenda, M., McDonnel, Y., McLean, L., Campbell, J., 2008. Unjust waters: climate change, flooding and the urban poor in Africa. Environ. Urban. 20 (1), 187–205. https://doi.org/10.1177/0956247808089156.

Eden, J.M., Widmann, M., 2014. Downscaling of GCM-simulated precipitation using model output statistics. J. Clim. 27 (1), 312–324.

Evans, J.P., Ji, F., Abramowitz, G., Ekström, M., 2013. Optimally choosing small ensemble members to produce robust climate simulations. Environ. Res. Lett. 8 (4), 1–4. https://doi.org/10.1088/1748-9326/8/4/044050.

Fowler, H., Kilsby, C., 2007. Using regional climate model data to simulate historical and future river flows in Northwest England. Clim. Chang. 80, 337–367. https://doi.org/10.1007/s10584-006-9117-3.

Fu, G., Charles, S.P., Chiew, F.H.S., Ekström, M., Potter, N.J., 2018. Uncertainties of statistical downscaling from predictor selection: equifinality and transferability. Atmos. Res. 203, 130–140. https://doi.org/10.1016/j.atmosres.2017.12.008.

Greve, P., Orlowsky, B., Mueller, B., Sheffield, J., Reichstein, M., Seneviratne, S.I., 2014. Global assessment of trends in wetting and drying over land. Nat. Geosci. 7, 716–721.

Guyon, I., Elisseeff, A., 2003. An introduction to variable and feature selection. J. Mach. Learn. Res. 3, 1157–1182.

Harris-J, E., 2001. Information Gain Versus Gain Ratio: A Study of Split Method Biases. The MITRE Corporation, Washington, Virginia.

Hay, L. E. and Clark, M. P. (2003) Use of statistically and dynamically downscaled atmospheric model output for hydrologic simulations in three mountainous basins in the western United States, J. Hydrol., 282, 56–75, doi:https://doi.org/10.1016/s0022-1694(03)00252-x,2003.

Hay, L.E., Wilby, R.J.L., Leavesley, G.H., 2000. A comparison of delta change and downscaled GCM scenarios for three mountainous basins in the United States. J. Am. Water Resour. Assoc. 36, 387–397. https://doi.org/10.1111/j.1752-1688.2000.tb04276.x.

Hertig, E., Seubert, S., Paxian, A., Vogt, G., Paeth, H., Jacobeit, J., 2014. Statistical modelling of extreme precipitation indices for the Mediterranean area under future climate change. Int. J. Climatol. 34, 1132–1156.

Houle, D., Bouffard, A., Duchesne, L., Logan, T., Harvey, R., 2012. Projections of future soil temperature and water content for three Southern Quebec forested sites. J. Clim. 25 (21), 7690–7701. https://doi.org/10.1175/JCLI-D-11-00440.1.

Immerzeel, W.W., Pellicciotti, F., Bierkens, M.F.P., 2013. Rising river flows throughout the twenty-first century in two Himalayan glacierized watersheds. Nat. Geosci. 6 (8), 1–4. https://doi.org/10.1038/ngeo1896.

Ishizaki, N., Dairaku, K., Ueno, G., 2017. Regional probabilistic climate projection for Japan with a regression model using multi-model ensemble experiments. Hydrol. Res. Lett. 11, 44–50. https://doi.org/10.3178/hrl.11.44.

Jiang, B.-N., Ding, X.Q., Ma, L.-T., He, Y., Wang, T., Xie, W.-W., 2008. A hybrid feature algorithm: combination of symmetrical uncertainty and genetic algorithm. In: The Second International Symposium on Optimization and Systems Biology (OSB'08) Lijiang, China, October 31– November 3.

Karewgowda, A.G., Manjunath, A.S., Jarayam, M.A., 2010. Comparative study of attribute selection using gain ratio and correlation based feature selection. Int. J. Inform. Technol. Knowled. Manag 2 (2), 271–277.

Khan, N., Shahid, S., Ahmed, K., Ismail, T., Nawaz, N., Son, M., 2018a. Performance assessment of general circulation model in simulating daily precipitation and temperature using multiple gridded datasets. Water 10 (12), 1793.

Khan, N., Shahid, S., Ismail, T., Wang, X.-J., 2018b. Spatial distribution of unidirectional trends in temperature and temperature extremes in Pakistan. Theor. Appl. Climatol. https://doi.org/10.1007/s00704-018-2520-7.

Knutti, R., Furrer, R., Tebaldi, C., Cermak, J., Meehl, G.A., 2010. Challenges in combining projections from multiple climate models. J. Clim. 23 (10), 2739–2758.

Lafaysse, M., Hingray, B., Mezghani, A., Gailhard, J., Terray, L., 2014. Internal variabilityand model uncertainty components in future hydrometeorological projections: the Alpine Durance basin. Water Resour. Res. 50, 3317–3341. https://doi.org/10.1002/2013WR014897.

Laflamme, E.M., Linder, E., Pan, Y., 2016. Statistical downscaling of regional climate model output to achieve projections of precipitation extremes. Weather Clim. Extr. 12, 15–23.

Li, J., Heap, A.D., Potter, A., Daniell, J.J., 2011. Application of machine learning methods to spatial interpolation of environmental variables. Environ. Model. Softw. 26, 1647–1659. https://doi.org/10.1016/j.envsoft.2011.07.004.

Liu, C., Alan, R.P., 2013. Observed and simulated responses in wet and dry season regions 1850–2100. Environ. Res. Lett. 8, 034002 11pp. https://doi.org/10.1088/1748-9326/8/3/034002.

Lutz, A.F., Maat, H.W., Biemans, H., Shrestha, A.B., Wester, P., Immerzeel, W.W., 2016. Selecting representative climate models for climate change impact studies: an advanced envelope-based selection approach. Int. J. Climatol. 36, 3988–4005. https://doi.org/10.1002/joc.4608.

Ma, C.-W., Ma, Y.G., 2018. Shannon information entropy in heavy-ion collisions. Prog. Part. Nucl. Phys. 99, 120–158.

Mahmood, R., Jia, S., 2017. An extended linear scaling method for downscaling temperature and its implication in the Jhelum River basin, Pakistan, and India, using CMIP5 GCMs. Theor. Appl. Climatol. 130, 725–734. https://doi.org/10.1007/s00704-016-1918-3.

Manzanas, R., Brands, S., San-Martín, D., Lucero, A., Limbo, C., Gutiérrez, J.M., 2015. Statistical downscaling in the tropics can be sensitive to reanalysis choice: a case study for precipitation in the Philippines. J. Clim. 28 (10), 4171–4184. https://doi.org/10.1175/JCLI-D-14-00331.1.

Maraun, D., Wetterhall, F., Ireson, A.M., Chandler, R.E., Kendon, E.J., Widmann, M., ... Venema, V.K.C., 2010. Precipitation downscaling under climate change: recent developments to bridge the gap between dynamical models and the end user. Rev. Geophys. 48 (3).

McSweeney, C.F., Jone, R.G., Lee, R.W., Rowell, D.P., 2015. (2015) Selecting CMIP5 GCMs for downscaling over multiple regions. Clim. Dyn. 44, 3237–3260. https://doi.org/10.1007/s00382-014-2418-8.
Merietu, T.S., Olarewaju, I.O., 2009. Resource conflict among farmers and Fulani herdsmen: implications for resource sustainability. Afr. J. Polit. Sci. Int. Relat. 3 (9), 360–364. Available online at. http://www.academicjournals.org/ajpsir, Accessed date: 20 October 2018.
Moron, V., Robertson, A.W., Ward, M.N., Ndiaye, O., 2008. Weather types and rainfall over Senegal, Part II: Downscaling of GCM simulations. J. Clim. 21, 288–307. https://doi.org/10.1175/2007jcli1624.1.
Nashwan, M.S., Shahid, S., 2018. Spatial distribution of unidirectional trends in climate and weather extremes in Nile river basin. Theor. Appl. Climatol. 1–19.
Nashwan, M.S., Shahid, S., Wang, X.-J., 2019. Uncertainty in estimated trends using gridded rainfall data: a case study of Bangladesh. Water 11 (2).
National Emergency Management Agency (NEMA), 2012. Worst Flooding in Decades. Releifweb. http://reliefweb.int/report/nigeria/worst-flooding-decades, Accessed date: 6 July 2018.
Ngene, B.U., Agunwamba, J.C., Nwachukwu, B.A., Okoro, B.C., 2015. The challenges to Nigerian rain gauge network improvement. Res. J. Environ. Earth Sci. 7 (4), 68–74.
Okoli, A.I.C., Atelhe, A.G., 2014. Nomads against Natives : a political ecology of herder/farmer conflicts in Nasarawa State, Nigeria. Am. Int. J. Contemp. Res. 4 (2), 76–88. Available: http://www.aijcrnet.com/journals/Vol_4_No_2_February_2014/11.pdf, Accessed date: 20 October 2018.
Oloruntade, A.J., Mohammad, T.A., Ghazali, A.H., Wayayok, A., 2017. Analysis of meteorological and hydrological droughts in the Niger-South Basin, Nigeria. Glob. Planet. Chang. 155, 225–233.
Onyutha, C., Tabari, H., Rutkowska, A., Nyeko-Ogiramoi, P., Willems, P., 2016. Comparison of different statistical downscaling methods for climate change rainfall projections over the Lake Victoria basin considering CMIP3 and CMIP5. J. Hydro Environ. Res. 12, 31–45.
Piani, C., Weedon, G.P., Best, M., Gomes, S.M., Viterbo, P., Hagemann, S., Haerter, J.O., 2010. Statistical bias correction of global simulated daily precipitation and temperature for the application of hydrological models. J. Hydrol. 395, 199–215. https://doi.org/10.1016/j.jhydrol.2010.10.024.
Piao, S., Ciais, P., Huang, Y., Shen, Z., Peng, S., Li, J., Zhou, L., Liu, H., Ma, Y., Ding, Y., Friedlingstein, P., Liu, C., Tan, K., Yu, Y., Zhang, T., Fang, J., 2010. The impacts of climate change on water resources and agriculture in China. Nature 467 (2), 43–51.
Pierce, D.W., Barnett, T.P., Santer, B.D., Gleckler, P.J., 2009. Selecting global climate models for regional climate change studies. Proc. Natl. Acad. Sci. U. S. A. 106 (21), 8441–8446. https://doi.org/10.1073/pnas.0900094106.
Pour, S.H., Harun, S.B., Shahd, S., 2014. Genetic programming for the downscaling of extreme rainfall events on the East Coast of Peninsular Malaysia. Atmosphere 5, 914–936.
Pour, S.H., Shahid, S., Chung, E.-S., Wang, X.J., 2018. Model output statistics downscaling using support vector machine for the projection of spatial and temporal changes in rainfall of Bangladesh. Atmos. Res. 213, 149–162.
Sa'adi, Z., Shahid, S., Chung, E.S., Ismail, T., 2017. Projection of spatial and temporal changes of rainfall in Sarawak of Borneo Island using statistical downscaling of CMIP5 models. Atmos. Res. 197, 446–460.
Sachindra, D.A., Huang, F., Barton, A.F., Perera, B.J.C., 2014. Multi-model ensemble approach for statistically downscaling general circulation model outputs to precipitation. Q. J. R. Meteorol. Soc. 140, 1161–1178. https://doi.org/10.1002/qj.2205.
Sachindra, D.A., Ahmed, K., Rashid, M.M., Shahid, S., Perera, B.J.C., 2018. Statistical downscaling of precipitation using machine learning techniques. Atmos. Res. 212, 240–258.
Salman, S.A., Shahid, S., Ismail, T., Chung, E.-S., Al-Abadi, A.M., 2017. Long-term trends in daily temperature extremes in Iraq. Atmos. Res. 198, 97–107. https://doi.org/10.1016/j.atmosres.2017.08.011.
Salman, S.A., Shahid, S., Ismail, T., Ahmed, K., Wang, X.-J., 2018. Selection of climate models for projection of spatiotemporal changes in temperature of Iraq with uncertainties. Atmos. Res. 213, 509–522.
Sanchez-Gomez, E., Somot, S., Déqué, M., 2009. Ability of an ensemble of regional climate models to reproduce weather regimes over Europe-Atlantic during the period 1961–2000. Clim. Dyn. 33, 723–736. https://doi.org/10.1007/s00382-008-0502-7.
Scherer, L., Pfister, S., 2016. Dealing with uncertainty in water scarcity footprints. Environ. Res. Lett. 11, 054008. https://doi.org/10.1088/1748-9326/11/5/054008.
Scherer, L., Verburg, P.H., 2017. Mapping and linking supply and demand side measures in climate smart agriculture. A review. Agron. Sustain. Dev. 37 (66). https://doi.org/10.1007/s13593-017-0475-1.
Schmidli, J., Frei, C., Vidale, P.L., 2006. Downscaling from GC precipitation: a benchmark for dynamical and statistical downscaling methods. Int. J. Climatol. 26, 679–689. https://doi.org/10.1002/joc.1287.
Schneider, U., Becker, A., Finger, P., Meyer-Christoffer, A., Ziese, M., Rudolf, B., 2014. GPCC's new land surface precipitation climatology based on quality-controlled in situ data and its role in quantifying the global water cycle. Theor. Appl. Climatol. 115 (1–2), 15–40.
Shannon, C.E. (1948) A mathematical theory of communication. Bell Syst. Tech. J., Vol. 27, pp. 379–423, 623–656.
Sharma, D., Das Gupta, A., Babel, M.S., 2007. Spatial disaggregation of bias-corrected GCM precipitation for improved hydrologic simulation: Ping River Basin, Thailand. Hydrol. Earth Syst. Sci. 11, 1373–1390. https://doi.org/10.5194/hess-11-1373-2007.
Shiru, M.S., Johnson, L.M., Ujih, O.U., Abdulazeez, O.T., 2015. Managing flood in Ilorin, Nigeria: Structural and Nonstructural measures. Asian J. Appl. Sci. 03 (05), 507–513.
Shiru, M.S., Shahid, S., Alias, N., Chung, E.-S., 2018. Trend analysis of droughts during crop growing seasons of Nigeria. Sustainability 10, 871. 13 pp. https://doi.org/10.3390/su10030871.
Shiru, M.S., Shahid, S., Chung, E.-S., Alias, N., 2019. Changing characteristics of meteorological droughts in Nigeria during 1901–2010. Atmos. Res. 223, 60–73. https://doi.org/10.1016/j.atmosres.2019.03.010.
Soraisam, B., Karumuri, A., Pai, D.S., 2018. Uncertainties in observations and climate projections for the North East India. Glob. Planet. Chang. 160, 96–108. https://doi.org/10.1016/j.gloplacha.2017.11.010.
Sorg, A., Huss, M., Rohrer, M., Stoffel, M., 2014. The days of plenty might soon be over in glacierized Central Asian catchments. Environ. Res. Lett. 9 (10). https://doi.org/10.1088/1748-9326/9/10/104018.
Spinoni, J., Naumann, G., Carrao, H., Barbosa, P., Vogt, J., 2014. World drought frequency, duration, and severity for 1951–2010. Int. J. Climatol. 34 (8), 2792–2804.
Steinschneider, S., McCrary, R., Mearns, L.O., Brown, C., 2015. The effects of climate model similarity on probabilistic climate projections and the implications for local, risk-based adaptation planning. Geophys. Res. Lett. 42, 5014–5022. https://doi.org/10.1002/2015GL064529.
Sun, F.B., Roderick, M.L., Lim, W.H., Farquhar, G.D., 2011. Hydroclimatic projections for the Murray-Darling Basin based on an ensemble derived from Intergovernmental Panel on Climate Change AR4 climate models. Water Resour. Res. 47, W00g02. https://doi.org/10.1029/2010wr009829.
Taylor, K.E., Stouffer, R.J., Meehl, G.A., 2012. An overview of CMIP5 and the experiment design. Bull. Am. Meteorol. Soc. 93, 485–498.
Thomas, V., López, R., 2015. Global increase in climate related disasters. In: Asian Development Bank (ADB) Economics Working Paper Series. No. 466.
Turco, M., Llasat, M.C., Herrera, S., Gutiérrez, J.M., 2017. Bias correction and downscaling of future RCM precipitation projections using a MOS-Analog technique. J. Geophys. Res. Atmos. https://doi.org/10.1002/2016JD025724.
Ubelejit, N.T., 2016. Fulani herdsmen and communal conflicts:climate change as precipitator. J. Polit. Sci. Leadership Res. 2 (1), 26–32.
Vetschera, R., Sarabando, P., Dias, L., 2014. Levels of incomplete information in group decision models - a comprehensive simulation study. Comput. Oper. Res. 51, 160–171.
Weezel, S.-V., 2017. Drought Severity and Communal Conflict in Nigeria. Available online. https://www.researchgate.net/publication/320374674_Drought_severity_and_communal_conflict_in_Nigeria, Accessed date: 20 October 2018.
WMO (World Meteorological Organisation), 1965. Guide to Hydro Meteorological Practice. WMO, Geneva (In: Ngene, B.U., Agunwamba, J.C., Nwachukwu, B.A., and Okoro, B.C. (2015) The challenges to Nigerian rain gauge network improvement. Research Journal of Environmental and Earth Sciences 7(4): 68–74).
Wood, A.W., Leung, L.R., Sridhar, V., Lettenmaier, D.P., 2004. Hydrologic implications of dynamical and statistical approaches to downscaling climate model outputs. Clim. Chang. 62, 189–216. https://doi.org/10.1023/B:CLIM.0000013685.99609.9e.
Xue, Y.K., Vasic, R., Janjic, Z., Mesinger, F., Mitchell, K.E., 2007. Assessment of dynamic downscaling of the continental U.S. regional climate using the Eta/SSiB regional climate model. J. Clim. 20, 4172–4193.
Yu, L., Liu, H., 2004. Efficient feature selection via analysis of relevance and redundancy. J. Mach. Learn. Res. 5, 1205–1224.